Supplement of Atmos. Meas. Tech. Discuss., 7, 8581–8642, 2014
http://www.atmos-meas-tech-discuss.net/7/8581/2014/
doi:10.5194/amtd-7-8581-2014-supplement

Atmospheric Measurement Techniques Discussions

Supplement of

Instrument inter-comparison of glyoxal, methyl glyoxal and NO_2 under simulated atmospheric conditions

R. Thalman et al.

Correspondence to: R. Volkamer (rainer.volkamer@colorado.edu)

27

Table S1: Correlation Matrix for experiment E1.[a]

Y↓ X→	CE-DOAS	BBCEAS	Mad-LIP	FT-IR [b]	W-DOAS	SPME	CE-DOAS[d]
CE-DOAS							
Slope							
Int[c]	-	1.032(2)	1.301(3)	1.02(3)	1.090(4)	1.05(12)	1.02(1)
R^2		0.005(2)	-0.06(2)	-0.1(7)	0.07(1)	0.01(1)	-0.17(1)
		0.9997	0.9998	0.999	0.9998	0.996	0.998
BBCEAS							
Slope	0.970(2)	-	1.2631 (8)	0.95(2)	1.048(1)	1.02(12)	0.97(1)
Int	-0.005(2)		-0.008(2)	0.5(6)	0.029(10)	0.00(2)	0.04(18)
R^2	0.9997		0.9998	0.997	0.9998	0.996	0.999
Mad-LIP							
Slope	0.768(2)	0.7917(5)	-	0.77(2)	0.836(1)	0.74(8)	0.77(1)
Int	0.06(2)	0.006(2)		0.2(4)	0.06(1)	0.03(1)	-0.05(18)
R^2	0.9998	0.9998		0.997	0.9994	0.995	0.9996
FT-IR [b]							
Slope	0.98(3)	1.05(2)	1.31(3)	-	1.07(2)	1.1(4)	1.03(10)
Int	0.1(7)	-0.6(6)	-0.3(5)		0.0(4)	-0.3(41)	-1(3)
R^2	0.999	0.997	0.997		0.999	0.96	0.998
W-DOAS							
Slope	0.917(3)	0.955(1)	1.197(2)	0.93(2)	-	0.93(10)	0.92(2)
Int	-0.06(1)	-0.028(9)	-0.07(2)	0.0(4)		-0.08(3)	-0.02(20)
R^2	0.9998	0.9998	0.9994	0.999		0.995	0.999
SPME							
Slope	0.95(10)	0.98(11)	1.35(15)	0.9(3)	1.07(12)	-	1.0(2)
Int	-0.01(1)	-0.00(2)	-0.04(2)	0.3(36)	-0.08(4)		0.0(14)
R^2	0.996	0.996	0.995	0.96	0.995		0.994
CE-DOAS[d]							
Slope	0.98(1)	1.04(1)	1.30(2)	0.97(10)	1.08(2)	1.0(2)	-
Int	0.17(10)	-0.05(19)	0.1(0.2)	1(3)	0.02(24)	0.0(14)	
R^2	0.998	0.999	0.9996	0.998	0.999	0.994	

[a] Number in parenthesis is the 1-σ fit error of the last displayed digit
[b] Correlations for high concentration data only
[c] Units of the intercept are ppbv
[d] CE-DOAS fitting for weak band range

28

Table S2: Correlation Matrix for experiment E8a.[a]

Y↓ X→	CE-DOAS	BBCEAS	Mad-LIP	FTIR	W-DOAS	SPME
CE-DOAS						
Slope	-	1.035(5)	0.919(4)	1.01(3)	1.092(8)	1.2(1)
Int b		0.013(3)	-0.011(3)	0.2(1)	0.08(2)	0.00(2)
R^2		0.9998	0.998	0.992	0.998	0.998
BBCEAS						
Slope	0.967(5)	-	0.9141(9)	0.95(2)	1.027(3)	1.1(1)
Int	-0.012(2)		-0.030(2)	0.0(1)	0.02(1)	-0.01(2)
R^2	0.9998		0.998	0.992	0.997	0.998
Mad-LIP						
Slope	1.088(4)	1.094(1)	-	1.02(2)	1.057(3)	1.3(1)
Int	0.012(2)	0.033(2)		-0.1(1)	-0.05(1)	0.01(1)
R^2	0.998	0.998		0.96	0.96	0.996
FTIR						
Slope	0.99(2)	1.05(2)	0.98(2)	-	1.08(2)	1.3(2)
Int	-0.2(1)	0.0(1)	0.1(1)		0.0(1)	-0.2(3)
R^2	0.992	0.992	0.96		0.987	0.994
White-cell DOAS						
Slope	0.916(7)	0.973(3)	0.946(3)	0.93(2)	-	1.1(1)
Int	-0.07(2)	-0.02(1)	0.05(1)	0.0(1)		-0.3(1)
R^2	0.998	0.997	0.96	0.987		0.998
SPME						
Slope	0.85(8)	0.88(9)	0.75(7)	0.8(1)	0.9(1)	-
Int	0.00(1)	0.01(1)	-0.009(10)	0.1(2)	0.3(1)	
R^2	0.998	0.998	0.996	0.994	0.998	

[a] Only data from daytime experiment with defined levels; [b] Intercept in ppbv;

30

Table S3: Correlation Matrix for the methyl glyoxal experiment E2.[a]

Y↓ X→	CE-DOAS	BBCEAS	Mad-LIP	FTIR	W-DOAS	PTR-MS
CE-DOAS						
Slope a	-	0.990(3)	0.714(3)	0.852(9)	1.03(3)	0.813(3)
Int		-0.35(2)	0.02(2)	-0.55(12)	0.0(3)	0.86(2)
R^2		0.9987	0.997	0.996	0.96	0.96
BBCEAS						
Slope	1.010(3)	-	0.720(3)	0.854(9)	1.05(3)	0.820(4)
Int	0.36(2)		0.38(3)	-0.02(10)	0.3(3)	1.25(3)
R^2	0.9987		0.996	0.994	0.96	0.96
Mad-LIP						
Slope	1.400(6)	1.388(6)	-	1.16 ± 0.02	1.45(5)	1.093(7)
Int	-0.03(3)	-0.53(4)		-0.6 ± 0.1	-0.2(4)	1.22(3)
R^2	0.997	0.996		0.995		0.96
FTIR						
Slope	1.174(13)	1.17(1)	0.86(1)	-	1.20(8)	1.04(3)
Int	0.65(13)	0.02(12)	0.5(1)		1.1(8)	0.3(2)
R^2	0.996	0.994	0.995		0.97	0.97
W-DOAS						
Slope	0.97(3)	0.95(3)	0.69(2)	0.84(6)	-	0.84(3)
Int	0.0(3)	-0.3(3)	0.1(3)	-0.8(7)		-0.3(4)
R^2	0.96	0.96	0.95	0.97		0.92
PTR-MS[b]						
Slope	1.231(5)	1.220(6)	0.915(6)	0.96(3)	1.19(4)	-
Int	-1.05(2)	-1.53(4)	-1.12(3)	-0.3(2)	0.4(4)	
R^2	0.96	0.96	0.96	0.97	0.92	

[a] Number in () is the 1 sigma standard deviation for the last reported digit [b] PTR-MS data filtered for ramp up and odd section that bumps higher than the trend in all of the other instruments and assumes a 5% uncertainty in the 1 minute PTR data.

31

32

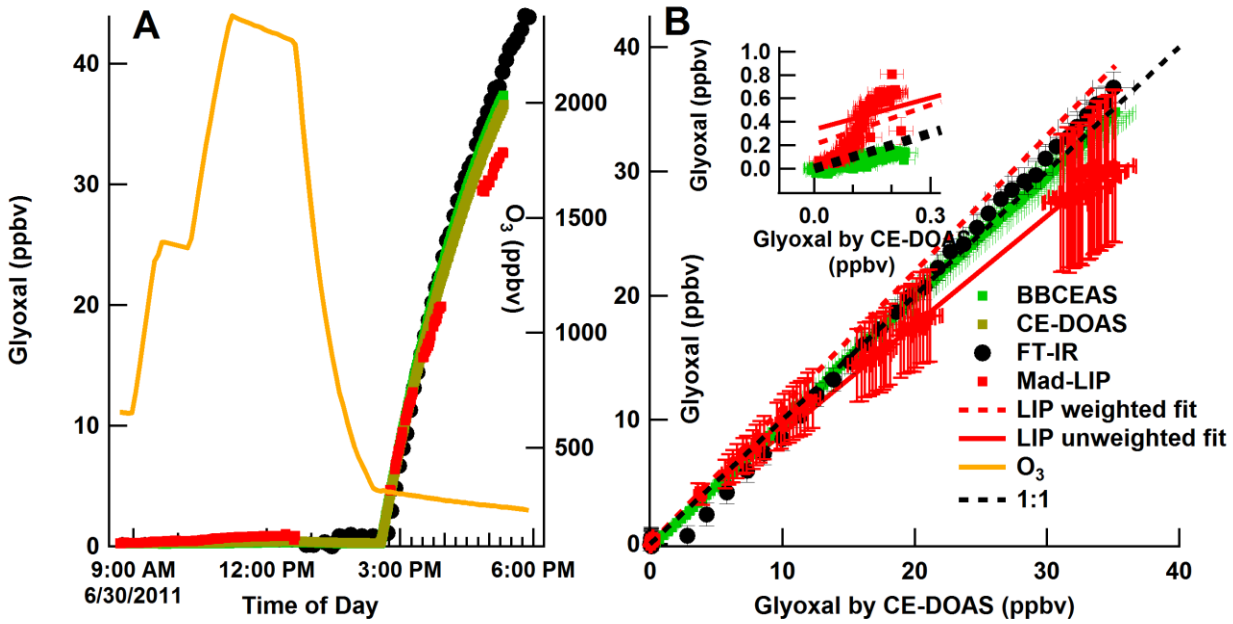

33

34 Figure S1: (A) Timeseries of glyoxal from E5. The morning consisted in stepping up the O_3
35 concentration in the chamber while varying the inlet tubing lengths to the various instruments.
36 O_3 was the flushed from the chamber till the concentration was ~250 ppbv after which C_2H_2 was
37 injected (20 ppmv). Glyoxal increases sharply once C_2H_2 is injected (14:32 UTC) into the
38 chamber containing O_3 (in absence of any TME). (B) Correlation plot for all glyoxal data, and
39 the low concentration points (inset), illustrating some evidence for non-linearity at high
40 concentrations, and bias at low concentrations that affected fitting of Mad-LIP data, but not the
41 other instruments. Fitting yielded an offset of 330 ± 20 pptv for an un-weighted linear fit, 205±3
42 pptv for Mad-LIP if a weighted linear fit and 220 ± 20 pptv if a 3rd order polynomial fit is
43 applied.

44

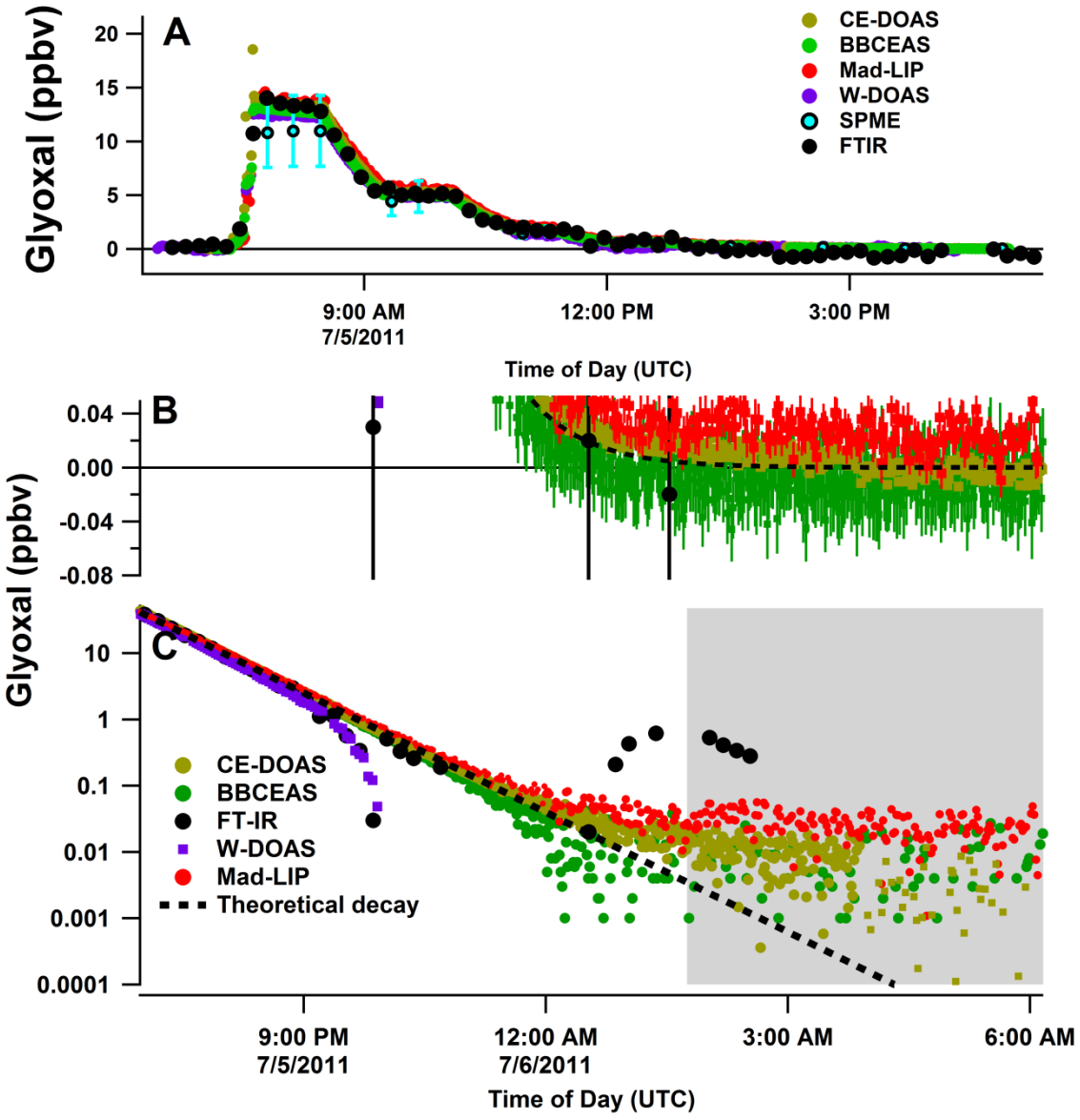

Figure S2: Time series of glyoxal experiment 8a (A). Overnight dilution experiment E8b (B and C). The decay of glyoxal in the chamber follows an exponential decay as the chamber is flushed. The data used for evaluating the detection limits and precision are taken from the (grey shaded) period between 2 AM and 6AM. Values below zero cannot be shown on the logarithmic plot in panel C; however, as panel B shows, the data were generally scattered around zero within the range of the instruments' detection limits.

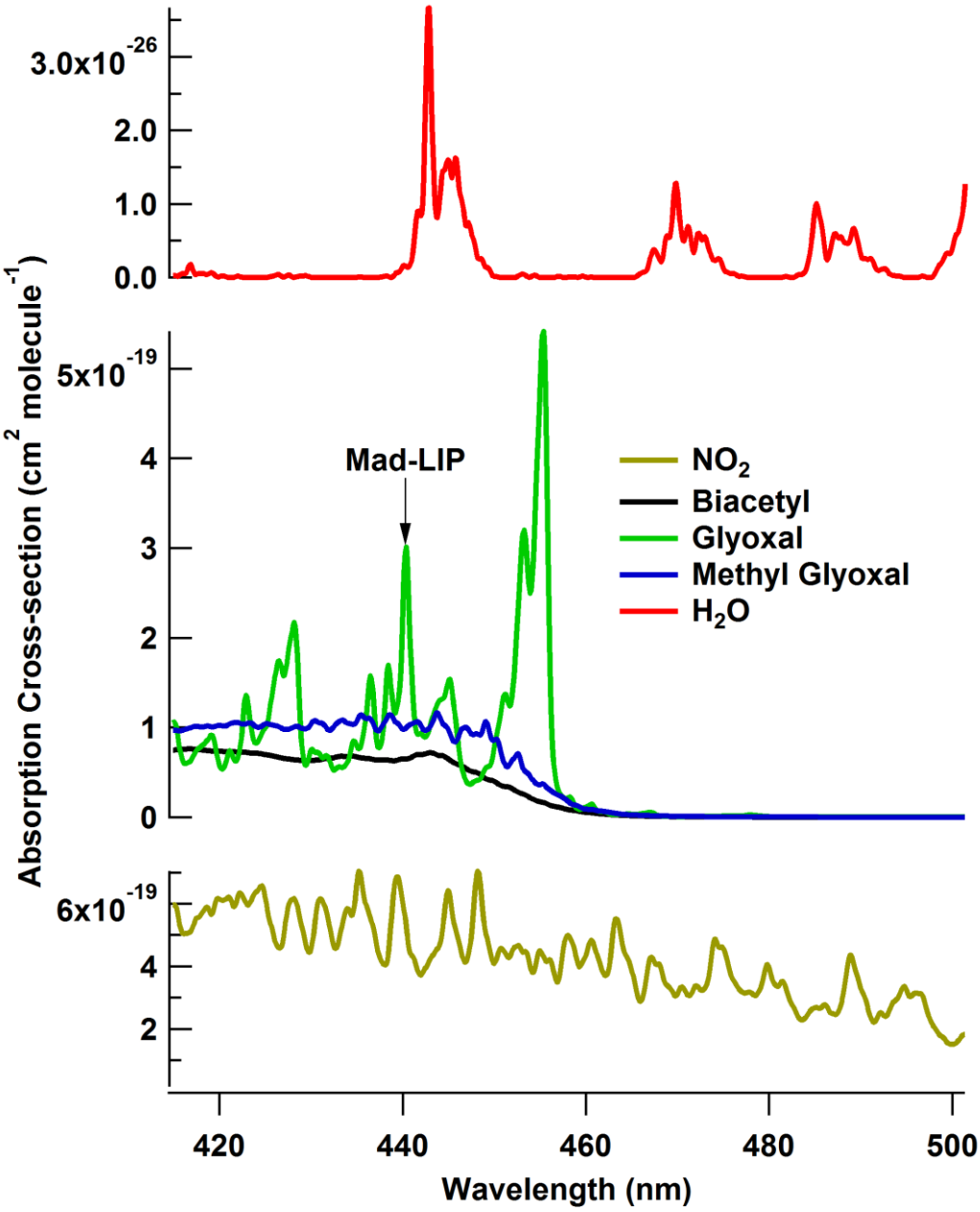

Figure S3: Absorption cross-sections of species measured by visible light absorption spectroscopy instruments (FWHM = 0.5 nm). NO_2 (Vandaele et al., 2002) and water (Rothman et al., 2009) absorb in the same region as glyoxal (Volkamer et al., 2005), methyl glyoxal (Meller et al., 1991) and biacetyl (Horowitz et al., 2001).

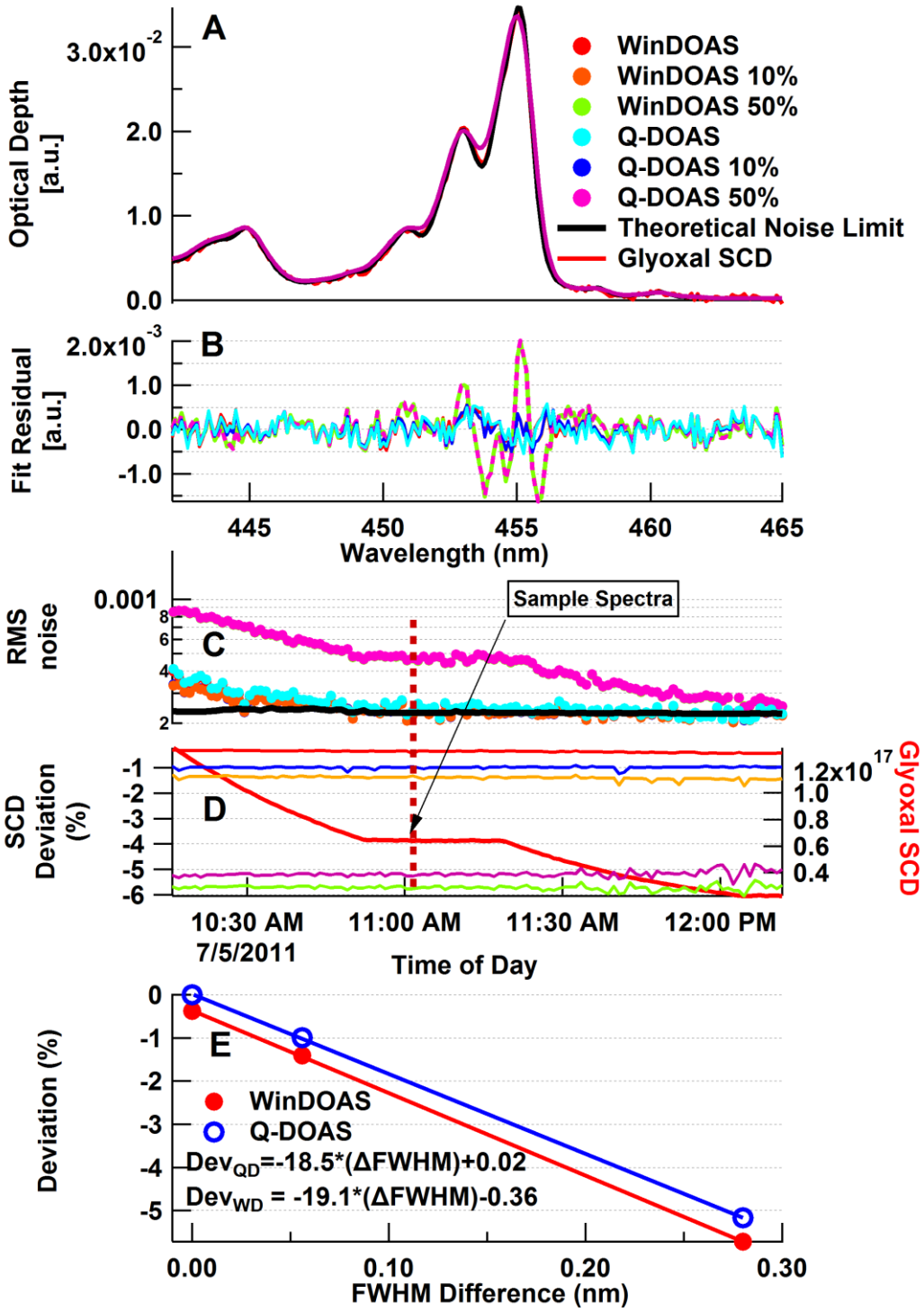

60

61 Figure S4: Sensitivity tests to quantify the small potential for calibration bias for glyoxal
62 measurements by CE-DOAS. See text for details.

63

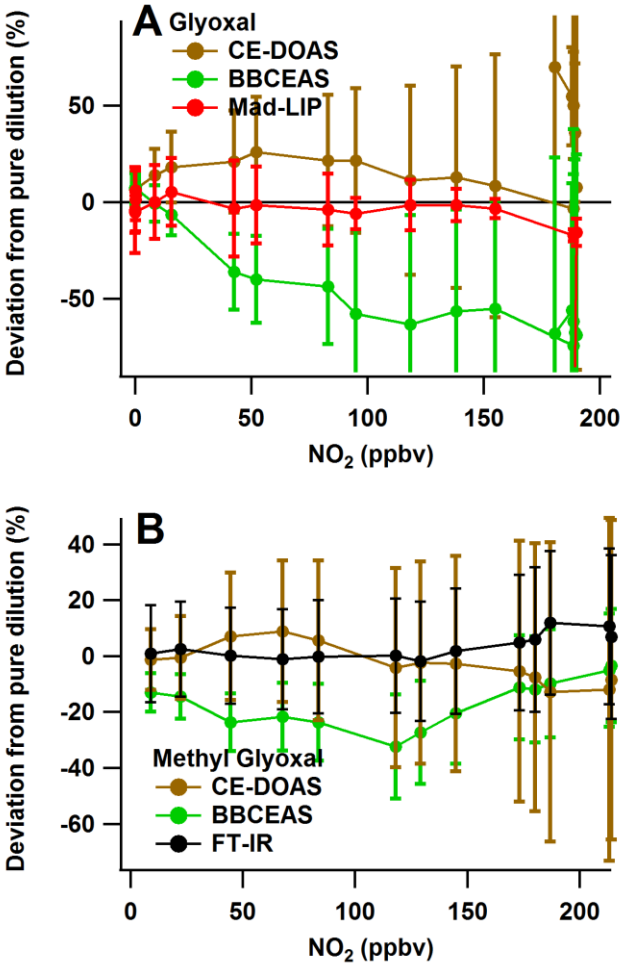

64

65 Figure S5: Deviations from pure dilution in the chamber for Experiments 9 and 10 relative to
66 NO_2 in the chamber. No clear trend is apparent over the full range of NO_2 investigated.

Description of CE-DOAS error propagation

The overall uncertainty of the CE-DOAS comes from a combination of the errors in the measurement. The contributing errors are as follows: Mirror Reflectivity (±2%), pressure measurement (±0.5% full scale range of pressure sensor), temperature (±0.01 K), physical lengths of the cavity (d_0, full cavity length 92.0±0.1cm; d_s, sample cavity length, 79±0.2 cm) and the absorption cross-sections (glyoxal, ±3% (Volkamer et al., 2005); NO_2 ±3% (Vandaele et al., 2002)). The relevant equations are as follows:

$$C_{gly} = SCD_{gly}/L_{eff} \quad \text{(S1)}$$

$$L(\lambda) = \frac{d_s}{1 - R(\lambda) + \alpha_{Ray}^{Air} d_0 + \sigma_{O_4} N_d{}^2 O_{2,mixing\,ratio}{}^2 d_s + \sigma_{NO_2} c_{NO_2} d_s} \quad \text{(S2)}$$

where the symbols and abbreviations are explained in the main text. In equation (S2) only the O_4 and NO_2 terms are considered to affect path length; a similar term could also be added for glyoxal self-limitation. The calculation is considered at a wavelength that has low O_4 absorption.

An initial value for the glyoxal (or NO_2) concentration is retrieved from Eq. (S1) using Eq. (S2) with no initial value for NO_2/glyoxal (Rayleigh case). For this case, the δL_{eff} = 1%. For high NO_2 cases (Experiments E9 and E10) the fit error for the SCDgly is on the order of 15% and dominates the error, regardless of the uncertainty in the cross-sections or the use of iterations. For the cases of glyoxal correlation experiments (Experiments E1 and E8a) the fit error is 1.5-2.0% over the full range of glyoxal concentrations investigated in absence of interfering species. At this low level of fit uncertainty the iterative solving of equations (S1) and (S2) to derive an accurate path begin to matter. We consider the first and second iteration, after which further iterations lead to changes smaller than 1 %.

Sensitivity tests: RMS noise and effect of convolution on CE-DOAS calibration

Fig. S4 makes an attempt to quantify the uncertainty in the calibration of CE-DOAS, and assess calibration bias due to transferring the literature cross-section to the actual instrument resolution (convolution). An example spectrum of glyoxal, recorded at 11am during E8a, is shown in panel (A); 1-3 ppbv, S/N = 180-300. The literature cross section was adjusted for resolution by convolution with the measured line function of a Kr atomic line emission lamp (FWHM = 0.56 nm @ 450.2 nm). Further tests were conducted, where the literature cross section was convoluted with an artificially broadened line function of 0.616 nm FWHM (10%) and 0.84 nm FWHM (50%). Tests were performed using two different convolution programs that are widely used in the DOAS community (QDOAS, WinDOAS (Fayt and Van Roosendael, 2001)). Panel (B) shows the fit residuals for the six cases investigated, that each used a different set of reference spectra. Panel (C) compares the time series of the retrieved RMS residual noise (1-sigma) for these case studies with the theoretical RMS noise that is expected for photon-shot noise limited

(white noise) spectra; see eq. (2) in Coburn et al. (2011). The RMS photon shot noise calculated for the specific case of the spectrum shown in (A) was 2.33×10^{-4} absorbance units (a.u.), which is near identical with the observed RMS = 2.39×10^{-4} a.u. RMS noise is indistinguishable (< 1%) for the $FWHM_{measued}$ and $FWHM_{10\%\text{-}bias}$ cases; significant residual structures remain for the $FWHM_{50\%\text{-}bias}$ case, for which the observed RMS is a factor of ~3 higher than $RMS_{shot\text{-}noise}$. The absence of systematic structures in the measured RMS, and the agreement with the RMS expected from theory demonstrate that the glyoxal absorption is well accounted for by CE-DOAS, and that the instrument is operating in the photon-shot noise limit.

We have quantified the effect of FWHM-bias on the retrieved SCD. Panel (D) shows the relative SCD deviation [calculated as 'deviation = $(SCD_{QDOAS} - SCD_X) / SCD_{QDOAS} * 100$']. Such deviations in the SCD are found to be much smaller than the effect on RMS. For the 50%-bias cases, the RMS increases by a factor of ~3, and SCD deviation is smaller 6%. Also shown is the glyoxal SCD, which varied by a factor of 5 over the time period shown here. The relative SCD deviation is independent of the glyoxal SCD. Finally, panel (E) shows that the relative SCD deviation is reasonably well approximated as a linear function of FWHM difference [= $FWHM_X$ – 0.56]. From the equation shown in Fig. 4E, and the uncertainty in our measured FWHM of 0.01 nm FWHM, we estimate that the overall bias from convolution of the literature cross-section to calibrate CE-DOAS spectra is less than ~0.5%.

The overall uncertainty in the CE-DOAS calibration is 3.5%, and dominated by the uncertainty in the literature cross section (~3%), with minor contributions from fit error (~1%), convolution (0.5%), and iterative solving for path lengths (1.5%). Based on the excellent agreement with the other instruments, we conclude that the possibility of other effects that can influence error (due to gas-transfer efficiencies, and sampling lines) do not appear to be limiting the overall error under the experimental conditions probed in this study.

References

Coburn, S., Dix, B., Sinreich, R., and Volkamer, R.: Development and Characterization of the CU Ground MAX-DOAS Instrument: lowering RMS noise and first measurements of BrO, IO, and CHOCHO near Pensacola, FL, Atmos. Meas. Tech., 4, 2421-2439, 2011.

Fayt, C. and Van Roosendael, M.: WinDOAS User Manual, 2001.

Horowitz, A., Meller, R., and Moortgat, G. K.: The UV–VIS absorption cross sections of the α-dicarbonyl compounds: pyruvic acid, biacetyl and glyoxal, J. Photochem. Photobio., A, 146, 19-27, 2001.

Meller, R., Raber, W., Crowley, J. N., Jenkin, M. E., and Moortgat, G. K.: The UV-visible absorption spectrum of methylglyoxal, J. Photochem. Photobio., A, 62, 163-171, 1991.

Rothman, L. S., Gordon, I. E., Barbe, A., Benner, D. C., Bernath, P. F., Birk, M., Boudon, V., Brown, L. R., Campargue, A., Champion, J. P., Chance, K., Coudert, L. H., Dana, V., Devi, V. M., Fally, S., Flaud, J. M., Gamache, R. R., Goldman, A., Jacquemart, D., Kleiner, I., Lacome, N., Lafferty, W. J., Mandin, J. Y., Massie, S. T., Mikhailenko, S. N., Miller, C. E., Moazzen-Ahmadi, N., Naumenko, O. V., Nikitin, A. V., Orphal, J., Perevalov, V. I., Perrin, A., Predoi-Cross, A., Rinsland, C. P., Rotger, M., Simeckovβ, M., Smith, M. A. H., Sung, K., Tashkun, S. A., Tennyson, J., Toth, R. A., Vandaele, A. C., and Vander Auwera, J.: The HITRAN 2008 molecular spectroscopic database, J. Quant. Spectrosc. Radiat. Transfer, 110, 533-572, 2009.

Vandaele, A. C., Hermans, C., Fally, S., Carleer, M., Colin, R., Merienne, M. F., Jenouvrier, A., and Coquart, B.: High-resolution Fourier transform measurement of the NO_2 visible and near-infared absorption cross sections: Temperature and pressure effects, J. Geophys. Res., 107, 4348, 2002.

Volkamer, R., Spietz, P., Burrows, J., and Platt, U.: High-resolution absorption cross-section of glyoxal in the UV-vis and IR spectral ranges, J. Photochem. Photobio., A, 172, 35-46, 2005.